ARTICLES

Measurement and calculation of the polarization transfer parameter $K_y^{y'}$ in neutron-deuteron scattering at 15.0, 17.0, 19.0, and 25.8 MeV

P. Hempen, P. Clotten, K. Hofenbitzer, T. Köble,* W. Metschulat, M. Schwindt, W. von Witsch,† L. Wätzold, and J. Weltz‡
Institut für Strahlen- und Kernphysik, Universität Bonn, D-53115 Bonn, Germany

W. Glöckle and D. Hüber§
Institut für Theoretische Physik II, Ruhr-Universität Bochum, D-44780 Bochum, Germany

H. Witała
Institute of Physics, Jagellonian University, Reymonta 4, PL-30059 Cracow, Poland
(Received 7 July 1997)

The nucleon-to-nucleon polarization transfer parameter $K_y^{y'}$ has been measured for the first time in neutron-deuteron scattering, at bombarding energies $E_n = 15.0$, 17.0, 19.0, and 25.8 MeV and scattering angles $\theta_{\rm lab} = 50°$ and 80°. The results are compared with rigorous, fully charge-dependent Faddeev calculations using the most recent realistic, phase-equivalent nucleon-nucleon interactions and the Tucson-Melbourne three-nucleon force (TM 3NF). Good agreement between theory and experiment was found at 50° where all potential models predict nearly the same value for $K_y^{y'}$. At 80°, the pure NN force predictions are spread due to their different D-state probabilities for the deuteron. When the TM 3NF is included, with the cutoff parameter in the strong form factors fitted to the experimental triton binding energy separately for each of the NN interactions, the different force predictions are shifted in such a way that they essentially agree with each other. This means that $K_y^{y'}$ scales with the triton binding energy. At 50°, the 3NF causes only a small decrease in the theoretical predictions, which still are close to the experimental values. In the minimum around 80°, the inclusion of the 3NF leads to a more pronounced decrease of $K_y^{y'}$ so that the theory now underestimates the data by about 10%. A comparison of our n-d data with existing p-d data indicates appreciable Coulomb force effects in the region of the minimum of $K_y^{y'}$. [S0556-2813(98)04802-X]

PACS number(s): 24.70.+s, 13.75.Cs, 21.45.+v, 25.40.Dn

I. INTRODUCTION

The experiment described in this paper was part of a program intended to investigate the isoscalar tensor force in the nucleon-nucleon (NN) interaction using polarized neutron beams.

An essential source of information on the tensor force, as well as all other components of the NN force, is deuteron properties and NN phase shifts determined by phase-shift analysis (PSA) of NN elastic scattering observables. PSA is a difficult procedure, which is reflected in quite different results for the NN phase shifts and mixing parameters obtained in the past. Even the two most recent and advanced multienergy PSA's of Stoks *et al.* [1] and of Arndt *et al.* [2], respectively, still show some differences in their results, especially in the $^3S_1$-$^3D_1$ mixing parameter ε_1, which is a direct measure of the on-shell tensor force. At 100 MeV, e.g., Arndt *et al.* get $\varepsilon_1 = 3.26$, while the result of the Nijmegen analysis is 2.42, with a quoted uncertainty of 0.09, clearly illustrating the need for more and better experimental data. (A comparison of the results and differences of these two PSA's for many phase shifts and energies can be found in Table 8 and Fig. 21 of Ref. [3].)

Differences in the results of PSA's arise because a PSA from a given restricted database is not unique. The mere fact that even the most recent NN potentials, with a common $\chi^2/N \approx 1$, lead to phase shifts which differ in a non-negligible way is a demonstration of this uncertainty: A different ansatz can lead to a different result. This is aggravated, of course, if the database is poor. Especially the tensor force, which involves the spins of both particles, is difficult to measure. Only a few n-p observables are sufficiently sensitive to allow the accurate determination of ε_1 at least in principle. They all involve polarized neutrons and necessitate the determination of the polarization of two of the reaction partners. This explains why, up to date, the tensor force is still only loosely constrained by the existing n-p data.

Looking for additional information about this force, the

*Present address: Fraunhoferinstitut für Naturwissenschaftlich-Technische Trendanalysen, D-53864 Euskirchen, Germany.
†Electronic address: vwitsch@iskp.uni-bonn.de
‡Present address: EFI, 2855 Campus Drive, San Mateo, CA 94403.
§Present address: Los Alamos National Laboratory, Theoretical Division, M.S. B283, Los Alamos, NM 87545.

next step naturally is to go to the $3N$ system. Here one finds that the triton binding energy E_t is sensitive to the tensor interaction. In fact, a weak tensor force seems to be needed below 50 MeV in order to bring potential model predictions for E_t into agreement with experiment [4]. However, the action of a three-nucleon force (3NF) can fill the gap between experiment and calculations for NN interactions with a stronger tensor force [5,6]. Unfortunately, the 3NF used most often up to now, the Tucson-Melbourne (TM) 3NF [7,8], has an ambiguity in the cutoff parameters Λ in the strong form factors. The Λ's can range within quite a large interval, causing strong variations in the $3N$ binding energy. This ambiguity is somewhat reduced by adding the π-ρ exchange to the π-π exchange [6]. Still, there are not yet consistent, predictive, and generally accepted NN and $3N$ forces, and the triton binding energy by itself does not allow one to distinguish which of the existing phase-equivalent NN forces is closer to reality. (See, however, the recent work in [9] which should be tested and applied in few-nucleon systems.)

A cheap but nevertheless informative way out of this unsatisfactory situation is to fit Λ to the experimental value of E_t and search for other observables in the $3N$ system which are sensitive to the tensor force. Such a quantity is the nucleon-to-nucleon spin transfer coefficient $K_y^{y'}$ whose sensitivity to the tensor force was pointed out in [10]. The comparison of rigorous Faddeev calculations with p-d measurements of $K_y^{y'}$ [11–14], however, was not conclusive because of three reasons.

First, the NN potentials available at that time had substantial on-shell differences, not only with respect to their predictions for the tensor force, but also in other phase parameters. In this respect, we are in a much better situation today because we now have four NN potentials at our disposal which all fit the same set of phase-shift parameters [1] with a χ^2 per datum very close to 1, namely, the phenomenological AV18 potential [15], the phenomenological Nijm I and Nijm II interactions [16,17], and the meson-theoretical CD-Bonn potential [18]. (The Nijm93 potential [16], which is also derived from meson theory, is fitted less perfectly.) Hereby Nijm II is purely local whereas Nijm I and AV18 carry a small nonlocality. The CD-Bonn potential, which is defined in momentum space, is strongly nonlocal. (Within this paper, we do not use the Nijm II interaction as published in [16] because it has an unphysical bound state in the $^1P_1$ wave at -964 MeV. Very recently, the $^1P_1$ wave of Nijm II was refitted [17] in order to remove this bound state.)

Second, the effect of 3NF's on $K_y^{y'}$ was not known at that time. A big step forward was achieved in [19,20] where, for the first time, a 3NF was included in rigorous calculations of the $3N$ continuum above the n-d break-up. Already there first calculations, using only S waves, showed that the inclusion of the TM π-π 3NF lowers the minimum of $K_y^{y'}$. Later we found [3] the same behavior for calculations including partial waves up to $j_{\max}=2$. In the meantime, we were able to include a 3NF in $3N$ continuum calculations even for very high angular momenta [21,22].

The third reason is the unknown effect of the Coulomb force on $K_y^{y'}$ in p-d scattering. The aim of the experiment described in this paper was to exclude this ambiguity. Therefore, taking advantage of the high intensity of our polarized neutron beam, we have measured $K_y^{y'}$ for the first time in n-d scattering, with an overall accuracy approaching that of typical p-d results. The measurements were made at bombarding energies $E_n=15.0$, 17.0, 19.0, and 25.8 MeV and scattering angles $\theta_{\rm lab}=50°$ and 80°. For $\theta_{\rm lab}$ around 80°, the theory predicts the strongest dependence of $K_y^{y'}$ on the tensor force and on the 3NF, while at forward angles these dependences vanish almost completely [3]. Already at 50°, the smallest angle accessible to our experiment, all models predict very similar values for $K_y^{y'}$ so that the data taken there can also be regarded as a check for systematic errors.

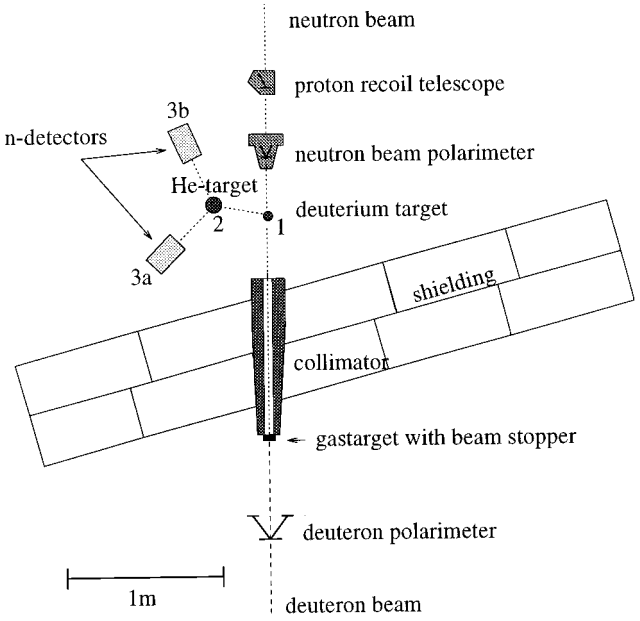

FIG. 1. Schematic drawing of the experimental setup, approximately to scale.

In the following section, the experimental setup and procedure will be described, and in Sec. III the data analysis by means of Monte Carlo simulations will be discussed. The Faddeev approach for the theoretical calculations will briefly be reviewed in Sec. IV, and the comparison with the experimental results will be presented in Sec. V. Finally, in Sec. VI, we summarize and give an outlook.

II. EXPERIMENTAL DETAILS

A. Polarized beam

The experiment was performed at the cyclotron of the Institut für Strahlen- und Kernphysik at the University of Bonn. A plan view of the experimental layout is shown in Fig. 1. The transversely polarized neutron beam was produced via the ^{2}H$(d,n)^3$He and ^{2}H$(d,n)pd$ reactions with 27.4-MeV vector-polarized deuterons incident on a 47-mm-long, liquid-nitrogen-cooled gas target operated at a pressure of 44 bars. The primary beam was stopped directly behind the gas target, which served as a Faraday cup. The neutrons were collimated at 0° in a 120-cm-long W-Cu collimator to form a circular beam with a diameter of 21 mm at the exit of the collimator and 30 mm at the position of the reaction target. The neutron production target and the neutron beam

have been described in detail elsewhere [23–25]. At an average intensity of the polarized deuteron beam of 400 nA, a collimated, quasimonoenergetic neutron flux of 1.3×10^6/s was obtained from the ^{2}H$(d,n)^3$He reaction—in the following called high-energy (HE) neutrons—with an average energy of 25.8 MeV and an energy spread of 4.4 MeV [full width at half maximum (FWHM)]. In addition, a large number of breakup neutrons (LE) was produced with energies below 21 MeV. Taking advantage of the fact that the high-energy part of this breakup continuum is also polarized [26], the usable beam intensity was effectively quadrupled by extending the measurement down to beam energies of around 14 MeV.

The polarization of the deuterons was measured with a carbon polarimeter positioned in front of the gas target. It was used mainly for tune-up of the atomic-beam ion source, and as a fast monitor during the runs. The actual neutron beam polarization was determined via n-α scattering in a chamber containing He gas at a pressure of 1 bar as well as two ΔE-E telescopes to detect recoil alpha particles at laboratory angles of $\pm24°$ with respect to the neutron beam, corresponding to the back-angle maximum in the n-α analyzing power at $\theta_n=119°$. The telescopes each consisted of a thin (30-μm) NE104 scintillator foil viewed from the outside by a photomultiplier (PM), a 450-mm^2 Si surface barrier detector, and a slit system. With this arrangement, the polarization of the neutrons could be measured for energies down to approximately 14 MeV. Although the efficiency of this polarimeter was only on the order of 10^{-8}, this was sufficient to determine the *average* neutron beam polarization over the long data runs with a statistical accuracy of about 1%. The neutron polarization was typically around 50% for both spin directions. Controlled by the current integrator, it was reversed approximately every 5 s by changing the polarization of the deuterons at the ion source. After each nine polarized cycles, a 5-s unpolarized measurement was inserted.

The intensity and energy distribution of the neutron beam were measured by means of a proton recoil telescope (PRT) placed behind the beam polarimeter. The neutron distribution as deduced from the PRT spectrum is shown in Fig. 2. The count rate in the quasimonoenergetic peak was used to determine the effective gas density in the n-production target. The beam energy was chosen such that the valley between the two neutron groups coincided with the n-α resonance at 22.1 MeV where the effective analyzing power of the beam polarimeter cannot be determined accurately. Neutrons between 20 and 23 MeV were not used for the analysis.

B. Target and polarimeter

The target consisted of a cylindrical, thin-walled glass vial, 35 mm high and 30 mm in diameter, filled with deuterated NE213 liquid scintillator [27] and sealed under nitrogen. It was viewed from below by a 2-in photomultiplier through a 10-mm-thick light guide. Ne213 was chosen for its excellent pulse-shape discrimination properties, which were mandatory for a good separation of elastic n-d scattering from breakup events. However, since the pulse shape of deuterons is not much different from that produced by protons, a special effort was still needed to obtain a useful p-d separation

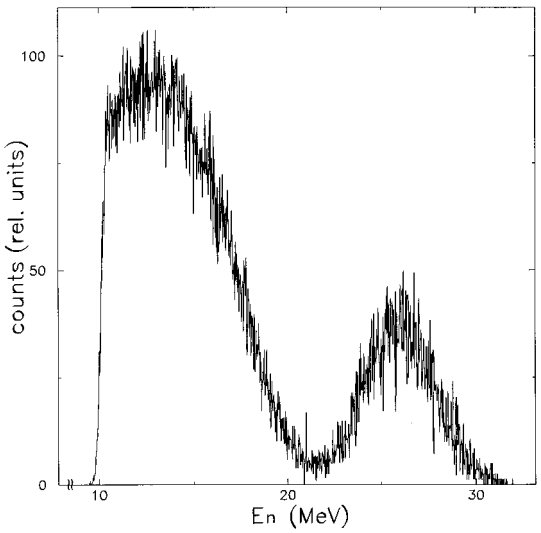

FIG. 2. Energy distribution of the neutron beam as measured with the proton recoil telescope. Recoils from neutrons below 10 MeV were stopped in the ΔE detector.

at free count rates of up to 1 MHz. After extensive studies the low-gain, eight-stage PM tube H2431 from Hamamatsu was chosen mainly for its very short anode-pulse rise time and high count-rate capability. The original high-current voltage divider was altered by lowering the voltage between the intermediate diodes to further reduce the anode current without appreciable degradation of the pulse quality. The resulting low gain was also necessary because the following fast electronics could not handle pulse heights exceeding ±2.5 V. Feedback regulation was applied to the anode voltage using a pulsed light-emitting diode (LED) to achieve optimum long-time gain stability.

The pulse-shape analysis was based on the principle of charge integration over different time regions of the anode pulse (''short-long'' method), using only commercially available general-purpose electronics [28]; a block diagram of the system is shown in Fig. 3. The anode signal was split, and one of the pulses was used to produce a timing signal for gating purposes. At this point, a fast coincidence with the main event trigger of the experiment reduced the free count

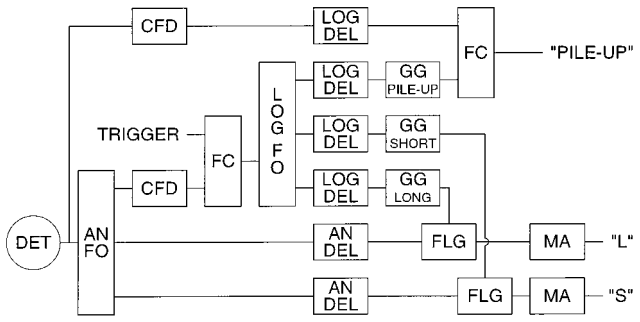

FIG. 3. Block diagram of the pulse-shape discrimination circuit. AN FO, analog fan-out; LOG FO, logic fan-out; CFD, constant fraction discriminator; FC, fast coincidence; GG, gate generator; FLG, fast linear gate; MA, main amplifier; TRIGGER, trigger from triple coincidence.

rate by about five to six orders of magnitude. The other two anode signals were fed into fast linear gates (PS744 [29]), which were opened for approximately 20 and 300 ns, respectively, by means of two logic units (PS755) serving as gate generators. By adjusting the delays, the short and long components of the anode pulse could thus be extracted. They were integrated and amplified with regular spectroscopy amplifiers. The pulse-shape resolution was optimized by fine-tuning the gate widths and positions. Pileup detection was incorporated through an additional ''long'' gate, which was started immediately after the fast component of the pulse and stayed open for the remaining duration of the pulse-shape analysis. If a second pulse was detected within this time period by a fast constant-fraction discriminator operating at a very low threshold, it was tagged as a pileup. This simple system worked very well and provided a good separation of protons and deuterons at count rates in the scintillator up to more than 500 kHz. As an example, Fig. 4 shows two scatter plots of the long vs short component. The same type of pulse-shape analysis was applied for n-γ discrimination in the n detectors.

The polarization of the scattered neutrons was determined with a liquid-He polarimeter. The LHe target consisted of a 120-mm-high steel cylinder of 80 mm diameter with 0.5-mm walls. It was closed at the bottom with a 5-mm-thick quartz window sealed with an O ring made from In wire. The inside walls were vapor coated with a thin film of Al in order to increase their reflectivity before a layer of 100 μg/cm^2 p,p'-diphenylstilbene (DPS) was deposited to shift the wave length of the LHe scintillation light from the ultraviolet into the visible region; for the window, a DPS thickness of 30 μm/cm^2 was chosen. The target cell was surrounded by a LN_2-cooled, cylindrical heat shield made of 0.3-mm-thick Al and closed at the bottom with a 5-mm-thick sapphire window. The vacuum jacket consisted of a steel cylinder of 128 mm diameter with a wall thickness of 1 mm. The target was viewed from below by a photomultiplier. The distance between the center of the deuterated target scintillator and the LHe cell was (300 ± 1) mm for the measurements at $\theta_{\rm lab}=80°$ and (374 ± 1) mm for those at 50°. Because of the close geometry of the experiment, the n-α scattering could only be observed at forward angles. Two 3-in thick NE213 liquid scintillator detectors in cylindrical BA1 cells [27] with 5-in diameter were positioned (320 ± 1) mm from the LHe target at $\theta_{n\alpha}=\pm(56.0\pm0.1)°$, which is close to the maximum in the analyzing efficiency of the polarimeter.

The n-d scattering data were written on magnetic tape if a fast triple coincidence was detected between the target scintillator (1), the LHe scatterer (2), and one of the n detectors ($3a$ or $3b$; see Fig. 1). For each event, the short and long components of the anode signals were recorded for the target and n detector together with the pulse height in the LHe scatterer, the time of flight between the target and LHe cell (TOF_{12}), the TOF from the LHe cell to the n detector (TOF_{23}), and the TOF of the incident neutron (TOF_{in}), using the radio frequency of the cyclotron as a stop signal. In the beam polarimeter, coincident ΔE-E signals were registered along with the TOF between the ΔE and E detector, and the TOF with respect to the rf of the accelerator. In addition, for each event the spin state of the beam was noted and, if applicable, the occurrence of pileup in the target.

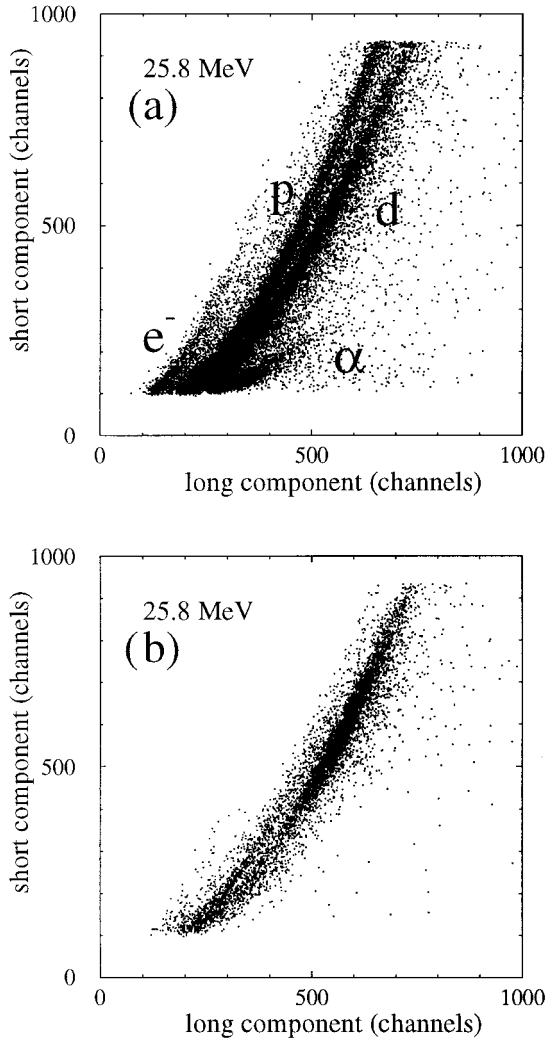

FIG. 4. Scatter plots of the long vs short component of the anode pulse from the deuterated target scintillator. In (a), the raw data are shown; the bands due to protons, deuterons, alphas, and electrons are labeled. In (b), the HE (25.8 MeV) neutrons were selected through a cut in TOF_{in}, and pileup was rejected in the target together with γ's in the n detector; in addition, a loose window was set about the true peak in the (TOF_{12} vs TOF_{23}) matrix [see Fig. 6(b)]. The island of HE recoil deuterons is now clearly visible, while breakup protons and low-energy deuterons are strongly suppressed.

Finally, in the proton recoil telescope, coincident ΔE-E signals were recorded.

III. DATA ANALYSIS

A. Formalism

For point geometry, the polarization of a neutron scattered to the left would be

$$p_{y'}^{n'}=(A_y^{nd}+p_y^nK_y^{y'})/(1+p_y^nA_y^{nd})$$

in a coordinate system where y and y' are along the normal to the scattering plane [30]. Primes denote the corresponding coordinates after scattering, A_y^{nd} is the analyzing power for n-d scattering and p_y^n is the neutron beam polarization. If we

define the asymmetry $a_n=(L-R)/(L+R)$, where L and R are the number of particles scattered in the polarimeter to the left and right, respectively, we obtain

$$a_n=p_{y'}^{n'}A_y^{n\alpha}.$$

Usually, L and R are replaced by a combination of count rates taken with different spin states of the beam in order to eliminate systematic errors [31], but even for a ''perfect'' experiment this asymmetry depends on A_y^{nd} in our case because the polarization of the scattered neutrons depends on this quantity. However, this unwanted influence of A_y^{nd} can be greatly reduced through an appropriate definition for the asymmetry. Denoting with L_+, L_-, L_0, R_+, R_-, and R_0 the count rates obtained with the beam polarization ''up,'' ''down,'' and ''zero,'' respectively, we define

$$a_n=\frac{2L_0R_0(L_+R_--L_-R_+)}{L_+L_-R_0^2+L_0R_0(L_+R_-+L_-R_+)+R_+R_-L_0^2}.$$

As explained in [32], a short measurement with unpolarized beam was necessary because the polarization for spin ''up'' and spin ''down'' was not exactly the same. Going through some lengthy algebra and omitting terms which are small compared with $(A_y^{nd})^2$ [33], this expression can be transformed into

$$a_n=A_y^{n\alpha}(p_y^++p_y^-)[K_y^{y'}-(A_y^{nd})^2],$$

which depends only on A_y^{nd} *squared* and on the *sum* of the absolute values of the beam polarizations measured with spin ''up'' (p_y^+) and spin ''down'' (p_y^-).

B. Monte Carlo simulations

1. General

The setup of this experiment constitutes a very ''poor'' geometry, and the formula derived above for point geometry cannot be used to extract $K_y^{y'}$ from the measured asymmetry. It is not possible to define an ''effective'' analyzing power for our polarimeter because, due to the angular dependence of the n-d and n-α scattering cross sections, the LHe target is not illuminated symmetrically so that the number of coincidences would be different for scattering to the left and scattering to the right even for unpolarized particles. Nevertheless, this formula can serve to demonstrate the basic connections between the various quantities and to estimate errors. The actual data analysis had to be done by means of detailed Monte Carlo simulations in which all aspects of the experiment were taken into account.

The simulation begins with the production of a polarized neutron at a random point in the gas target and follows it through the n-d and n-α scattering processes until it is finally recorded in one of the n detectors. In the course of the simulation, list-mode data were created which could be compared with the corresponding experimental spectra.

In order to calculate the neutron polarization after n-d scattering, a preliminary assumption had to be made about the magnitude of the spin-transfer parameter. For this, the predictions of rigorous Faddeev calculations [34] with various realistic N-N potentials were used. The asymmetry a_n was then determined from the simulated ''left'' and ''right'' counting rates, and compared to the measured one. If the two differed, the simulation was repeated with somewhat larger or smaller values of $K_y^{y'}$ until agreement was obtained. At this point, obviously, the *assumed* distribution of $K_y^{y'}(\theta)$ describes the experiment correctly, and the value *at the central bombarding energy and scattering angle* was taken as the ''experimental'' result. This procedure is reasonable because, even though the *absolute value* of $K_y^{y'}$ may change for different potential models, the basic *shape* of the angular distributions remains always the same (see Fig. 7).

Out-of-plane scattering was significant in this experiment so that the effective beam polarization could have a noticeable x component. Consequently, $K_x^{x'}$ was also needed in the simulation. The only experimental information available on this quantity is from a proton-deuteron measurement at 10 MeV [13]. In order to estimate the error introduced by this uncertainty, simulations were done in which the theoretical predictions for $K_x^{x'}$ were changed by up to 30%; the effect on $K_y^{y'}$ was found to be negligible. Also negligible was the effect of a possible deviation by a few degrees of the spin direction from the normal to the scattering plane.

In order to assess the effects of energy and angular smearing in this experiment, the simulation was repeated for point geometry, assuming monoenergetic beams and small targets and detectors. The resulting change in a_n was 6.5% for the measurement at 50° and 7.5% at 80°.

Multiple-scattering effects were investigated in a separate program. The most important correction to the measured asymmetry was due to scattering from foreign materials surrounding the LHe target which could change the asymmetry by as much as 1% at the lowest energy, while double scattering in the LHe itself contributed only around 0.2%. Also significant was double scattering in the deuterium target, with a contribution of up to 0.5%. These effects, however, could be calculated very accurately. Double scattering in the target involving carbon or other elements was much less serious, and triple scattering could be ignored completely. Taken all together, multiple scattering lowered the asymmetry by 1.3% at $\theta_{\rm lab}=50°$ and by 2.3%–2.8% at $\theta_{\rm lab}=80°$, depending on the energy.

In order to calculate the asymmetries for the LE part of the neutron beam, simulations were needed to find the energy distribution of the incident neutrons corresponding to a given cut in $\mathrm{TOF_{in}}$. A final goal of the Monte Carlo calculations was to estimate the influence of systematic errors of various experimental quantities such as the target and detector positions and beam parameters. Corresponding simulations were made for the beam polarimeter to determine its effective analyzing power.

2. Input data

Because of the extended geometry and because of multiple scattering, a vast amount of input data was needed for the Monte Carlo simulations, covering a large range of energies and angles. Of these, the n-α analyzing powers were, of course, the most important ones. For the beam polarimeter, $A_y^{n\alpha}$ was needed only in the well-determined back-angle maximum around $\theta_{\rm c.m.}=132°$. For the energies around 25.8 MeV, the phase shifts of Broste *et al.* [35] and Krupp *et al.*

[36] were used, and below 20 MeV those of Stammbach and Walter [37]. Two very accurate p-α calibration points exist at 17 MeV [38] and at 26 MeV [39], respectively, which can be used to check the n-α data as demonstrated by Krupp *et al.* [36]. In both cases, the n-α phase-shift prediction agrees very well with the p-α calibration point. The total absolute error in the effective analyzing power $A_{\rm eff}^{n\alpha}$ of our beam polarimeter, including systematic errors and background corrections, is estimated to be $\pm 1.3\%$ at 25.8 MeV and 1.1% at the lower energies.

The polarization of the scattered neutrons, as mentioned in Sec. II B, was determined by n-α scattering at forward angles around 56°. In this region, for energies above 7–8 MeV, the existing phase-shift predictions for $A_y^{n\alpha}$ differ appreciably [37,40], meaning unacceptable normalization errors mainly for the measurement at $\theta_{\rm lab}=50°$ where the energy of the scattered neutrons is highest. We have therefore remeasured $A_y^{n\alpha}$, combined our data with those of other authors, and concluded that the phase shifts of Stammbach and Walter [37] describe the n-α analyzing power very well at all angles and energies. The results of these investigations will be described in detail in a separate paper [41]. The n-α cross sections were calculated from phase shifts in all cases.

Whereas the differential cross section for n-d scattering is very well reproduced by modern three-nucleon calculations, the analyzing power for energies below 30 MeV is not [42]. Consequently, A_y^{nd} was interpolated from measured data of various authors [43], and an absolute error of 10% was assumed for this quantity. The cross sections for elastic n-C scattering were taken from the compilation ENDF/B-VI [44]; inelastic processes were negligible. For energies below 12 MeV, polarization data for n-C scattering were calculated from phase shifts [45]; above 12 MeV optical-model predictions were used [46]. For double scattering involving other elements such as Fe, Al, O, and Si, cross sections from [44] were used, but polarization effects were neglected. This could safely be done because these contributions were very small.

IV. THEORETICAL APPROACH

The Faddeev equation for the $3N$ continuum which we are using, and which is based on NN forces only, reads

$$T = tP + tG_0PT, \tag{1}$$

where t is the NN t matrix, G_0 the free $3N$ propagator, and P the sum of a cyclic and an anticyclic permutation of the three nucleons. We solve this integral equation for the Faddeev amplitude T in momentum space rigorously and with very high numerical accuracy [47]. The transition operator U for elastic n-d scattering is given by quadrature as

$$U = PG_0^{-1} + PT. \tag{2}$$

In the calculations using NN forces only, we include charge dependence as described in [48]. Because of the uncertainty in the n-n force, we replace it in our calculations by the p-p force and thus neglect charge-symmetry breaking.

In order to include a 3NF, one can also work with only a single Faddeev equation as was shown recently in [21]:

$$\widetilde{T} = tP + (1+tG_0)V_4^{(1)}(1+P) + tG_0P\widetilde{T} + (1+tG_0)V_4^{(1)}(1+P)G_0\widetilde{T}. \tag{3}$$

This equation has an additional driving term and an additional integral kernel in comparison with Eq. (1). The new quantity in Eq. (3) is $V_4^{(1)}$, which is a part of the full 3NF V_4:

$$V_4 = V_4^{(1)} + V_4^{(2)} + V_4^{(3)}. \tag{4}$$

Hereby we made use of the fact that 3NF's used up to now naturally split into three parts, each of them being symmetric under the exchange of two of the three particles, e.g., $V_4^{(1)}$ under exchange of particles 2 and 3. Now the elastic transition operator is given by

$$U = PG_0^{-1} + P\widetilde{T} + V_4^{(1)}(1+P) + V_4^{(1)}(1+P)G_0\widetilde{T}. \tag{5}$$

For the numerical treatment of the new terms in Eqs. (3) and (5), see [19] and [20].

Important in this context is the calculation of the matrix elements of $V_4^{(1)}$. As was shown recently in [22], the partial wave decomposition for $V_4^{(1)}$ used up to now [19] is accurate in the lower partial waves where we use it, but leads to untractable numerical problems in the higher ones. Therefore, we introduced in [22] a new scheme for the partial wave decomposition of the 3NF which is stable in all partial waves. This allows for the calculations presented in this paper to include a sufficiently high number of partial waves for the 3NF to achieve converged results. For the first time, we present calculations including a 3NF for the $3N$ continuum above the breakup threshold including partial waves with a two-body total angular momentum $j=3$, whereas in the $3N$ bound state calculations [49], which we performed in order to fit Λ, we went up to $j_{\rm max}=6$. For the calculations including a 3NF, we again consider charge dependence, but for the sake of simplicity, we neglect the channels with total isospin $T=3/2$. Without 3NF's, this was shown to be justified in [3].

V. RESULTS AND DISCUSSION

In five runs comprising approximately 1800 h of data taking, 1.1 C of charge were collected for the measurements at $\theta_{\rm lab}=80°$ and 0.6 C at $\theta_{\rm lab}=50°$. To obtain the beam polarization, the matrices $\mathrm{TOF_{in}}$ vs E and E vs ΔE were used (Fig. 5). After the application of appropriate windows, mainly to eliminate deuterons from the $^4\mathrm{He}(n,d)^3\mathrm{H}$ reaction, the spectra were very clean with little accidental background. The average sum of the beam polarizations was $(p_y^+ + p_y^-) = 1.042 \pm 0.009$ for the quasimonoenergetic peak at $E_n = (25.8 \pm 2.2)$ MeV and 0.983 ± 0.008 for the breakup continuum between 14 and 20 MeV, where the errors are statistical only. Thus the polarization in the upper part of the breakup continuum is 6% lower than that in the high-energy peak, in good agreement with an earlier measurement [26]. Only a very small energy dependence of the polarization was found in the low-energy region investigated.

In order to obtain the asymmetry for the scattered neutrons, two-dimensional windows were first applied in the pulse-shape matrices to remove coincidences where a

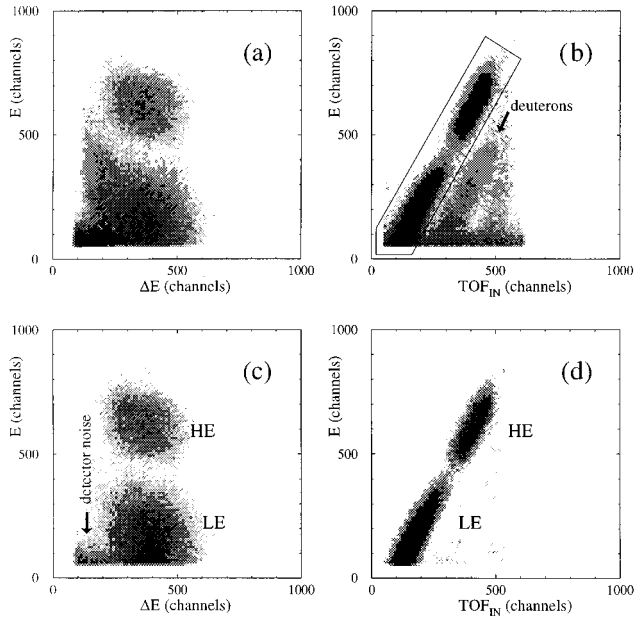

FIG. 5. Matrices (TOF$_{in}$ vs E) and (E vs ΔE) for the beam polarimeter. In (a) and (b) the raw data are shown, and the arrow indicates deuterons from the ^{4}He$(n,d)^3$H reaction; (c) shows the (E vs ΔE) matrix with the window indicated in (b) applied to the (TOF$_{in}$ vs E) matrix. (d) is the (TOF$_{in}$ vs E) matrix with a cut in ΔE at channel 250 to eliminate most deuterons and detector noise. The peak from channel 450–770 is due to the (HE) neutrons from the ^{2}H$(d,n)^3$He reaction; below channel 400 are the events originating from the (LE) breakup continuum.

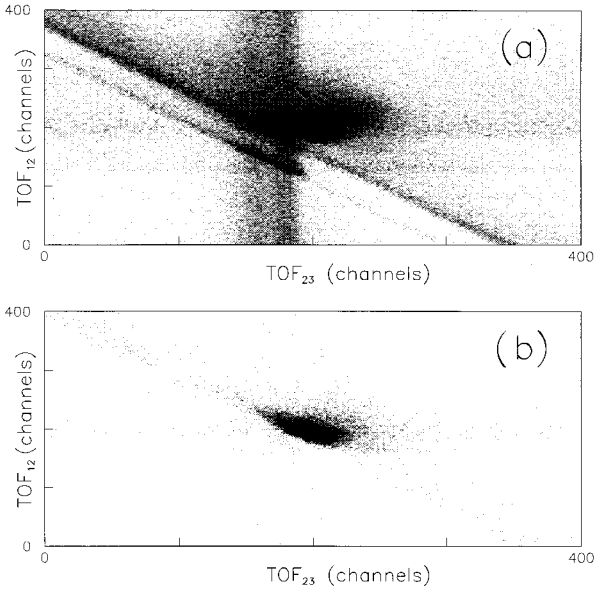

FIG. 6. Example of a (TOF$_{12}$ vs TOF$_{23}$) matrix before (a) and after (b) elimination of background events through pulse-shape windows in detectors 1 and 3, for E_n=25.8 MeV and θ_{lab}=80°. The intensity scale is logarithmic in both pictures in order to enhance the areas with low count rates. The events to the right of the ''true'' peak in (b) are mainly due to multiple scattering and some breakup. The time scales are 0.16 ns/channel.

gamma was detected in one of the n detectors. Then, besides the quasimonoenergetic region at 25.8 MeV, three groups of breakup neutrons were selected in the n beam with mean energies of 15, 17, and 19 MeV, respectively, by placing the appropriate cuts in the TOF$_{in}$ spectrum as determined by the Monte Carlo simulation. In the next step, a window was set about the recoil deuterons in the pulse-shape matrix of the target scintillator (Fig. 4). In the 25.8-MeV energy bin, roughly 90% of all breakup protons were thereby cut out and most of the rest were eliminated by windows in the TOF matrices (see Fig. 6). Since the elastic n-d coincidences are more localized in time than the breakup events, only about 10% of these fall inside the ''elastic'' windows so that the final background from breakup was in the order of 1%. For this a correction was made which resulted in an additional error in the asymmetry of 0.2%. For the lower beam energies, the quality of p-d separation was not so good. However, because the *relative* number of breakup events was smaller at lower energies and because their asymmetry could be determined rather accurately, the error resulting from breakup subtraction here remained tolerable at $<1\%$. The same TOF matrices were used to remove accidental background by subtracting the counts in corresponding windows which were shifted by one rf period into the regions of negative TOF. At free counting rates of 200 kHz in the target scintillator, 10 kHz in the LHe target, and 30 kHz in the n detectors, the number of accidentals after pulse-shape selection was always less than 0.5%. The relative number of multiple-scattering events inside the ''elastic'' windows was determined by the Monte Carlo simulation. Their effect on the asymmetry has been discussed in Sec. III B.

The final results, after subtraction of background and correction for double scattering, are listed in Table I together with their relative errors. The normalization uncertainty for $K_y^{y'}$ at the three lower beam energies is 1.8%. Since at these energies the same set of phase shifts could be used to determine the neutron polarization before and after scattering, the normalization errors of $A_y^{n\alpha}$ partly cancel out [41]. At 25.8 MeV the situation is different: Here the beam energy is above the $3/2^+$ n-α resonance, while the neutron energies after scattering are below it, so that different sets of phase shifts had to be used to determine the two analyzing powers and their respective errors add. For this case, we assign an overall normalization uncertainty of 2.4%. The individual

TABLE I. Results for the asymmetry a_n and the spin-transfer parameter $K_y^{y'}$. The errors represent one standard deviation and are mainly due to counting statistics and uncertainties in the various corrections. The scale errors for $K_y^{y'}$ are not included; they are estimated to be 1.8% at the three lower energies and 2.4% at 25.8 MeV.

E_n (MeV)	θ_{lab}	$-a_n$	$K_y^{y'}$
15.0	50°	0.386±0.005	0.804±0.022
	80°	0.375±0.004	0.632±0.015
17.0	50°	0.376±0.005	0.826±0.022
	80°	0.355±0.005	0.608±0.016
19.0	50°	0.346±0.013	0.807±0.036
	80°	0.330±0.009	0.583±0.020
25.8	50°	0.325±0.007	0.813±0.024
	80°	0.280±0.009	0.535±0.019

TABLE II. Individual contributions to the total error of $K_y^{y'}$ at 17.0 and 25.8 MeV, for $\theta_{lab}=80°$. The errors at 15.0 and 19.0 MeV are similar to the ones at 17.0 MeV.

	$\Delta K_y^{y'}/K_y^{y'}$ (%)	
Source of error	$E_n=17.0$ MeV	$E_n=25.8$ MeV
LHe polarimeter		
Counting statistics (experiment)	1.3	3.0
Statistics (Monte Carlo)	0.2	0.2
Background subtraction (accidental)	0.2	0.2
Background subtraction (breakup)	0.9	0.3
Multiple-scattering correction	0.8	0.8
Neutron beam (mean energy)	0.9	0.1
Uncertainty in $A_y^{n\text{-}d}$ ($\pm 10\%$)	0.2	0.6
Relative systematic errors (geometry)	1.0	1.1
Absolute normalization of $A_y^{n\text{-}\alpha}$	1.8[a]	2.0
Beam polarimeter		
Counting statistics	0.9	1.1
Background subtraction	0.5	0.2
Systematic errors (geometry)	0.1	0.1
Other experimental parameters	0.2	0.2
Absolute normalization of $A_y^{n\text{-}\alpha}$	a	1.3
Total error (%)	3.1	4.3

[a]For a discussion of the normalization error for the three lower beam energies, see the main text.

contributions to the total errors are detailed in Table II for the measurements at 17.0 and 25.8 MeV and $\theta_{lab}=80°$.

In a first study, we compare our results in Fig. 7 with charge-dependent calculations based on *NN* forces only, as described in the previous section. We used the four phase-equivalent potentials AV18 [15], Nijm I and II [16,17], and CD-Bonn [18], including all partial waves up to a two-body angular momentum $j_{max}=3$. At this point it should be emphasized that our experimental results for $K_y^{y'}$ were obtained via comparison with Monte Carlo simulations, as explained in Sec. III B, and represent the values at the exact energies and angles indicated; they can therefore directly be compared with theory. It is gratifying to find good agreement at $\theta_{lab}=50°$ where the theoretical predictions do not depend much on the energy or on the particular potential model used. On average, the 50° data agree with theory within 1.2%.

At $\theta_{lab}=80°$, which is close to the minimum at all four energies, we find the strongest variation among the predictions of the four *NN* potentials. While AV18, Nijm I, and Nijm II are within the experimental errors at all energies, the CD-Bonn prediction is distinctly lower. As shown in Table III, these variations in the minimum of $K_y^{y'}$ are related to the different strengths of the tensor force of the *NN* potentials as expressed by their respective *D*-state probabilities P_D. It can be seen from Table III that the value of $K_y^{y'}$ at $\theta_{lab}=80°$ increases with the strength of the tensor force. Thus, judging from Fig. 7, one might conclude that our data at $\theta_{lab}=80°$ prefer the potentials with a stronger tensor force over the CD-Bonn potential, which has the lowest P_D. However, as detailed below, this simple picture, which was initially believed to provide direct information on the tensor force

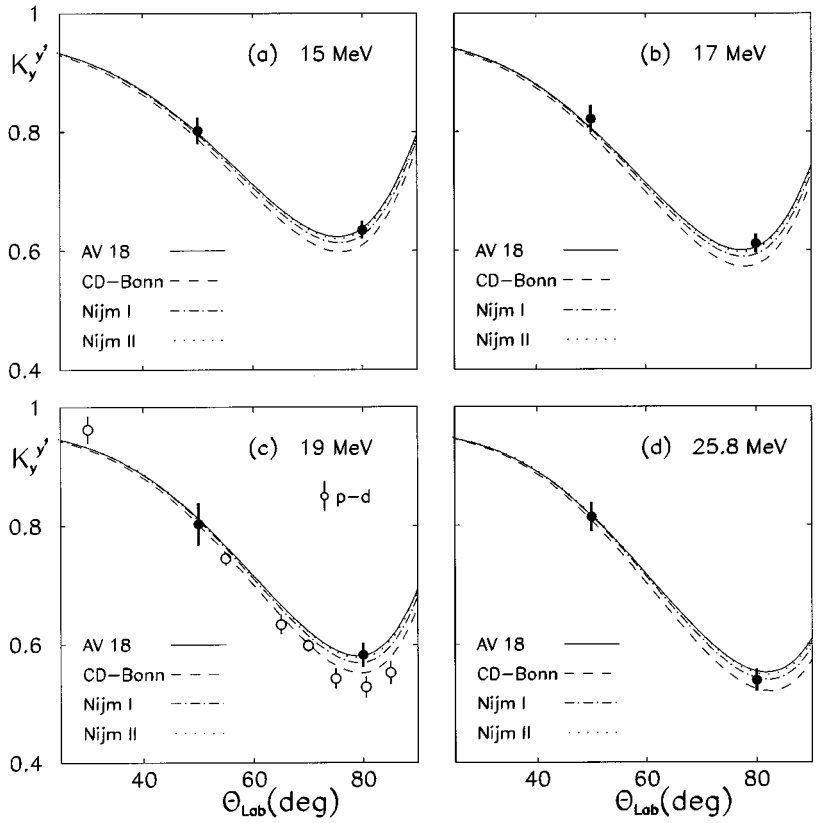

FIG. 7. Experimental results for $K_y^{y'}$ for the four beam energies measured, in comparison with the predictions of rigorous Faddeev calculations with various realistic, phase-equivalent *NN* potentials. The solid line is for the AV18 potential [15], the dashed one for the CD-Bonn potential [18], and the dash-dotted and dotted lines are for Nijm I and II [16], respectively. The solid dots are the results of the present experiment; the vertical bars indicate the relative errors. In (c), at $E_n=19$ MeV, the open circles represent the *p-d* data of Sydow *et al.* [14], taken at the same energy.

TABLE III. Deuteron D-state probability in comparison with the triton binding energy E_t and the values of $K_y^{y'}$ at $\theta_{\rm lab}=80°$, which is close to the minimum at all energies, for the four realistic and phase-equivalent potentials used in this paper.

			$K_y^{y'}(80°)$ at E_n (MeV)			
Potential	P_D (%)	E_t (MeV)	15.0	17.0	19.0	25.8
AV18	5.78	7.58	0.640	0.606	0.582	0.553
Nijm I	5.68	7.73	0.629	0.594	0.570	0.542
Nijm II	5.65	7.71	0.637	0.603	0.579	0.550
CD-Bonn	4.83	7.95	0.612	0.577	0.552	0.523

[3,11,14], must be modified when three-nucleon forces are included.

At 19 MeV we also show the p-d data of Ref. [14], taken at the same energy. They agree with our n-d result at $\theta_{\rm lab}=50°$, but are about 10% below the n-d point in the minimum. The same behavior is observed for another p-d measurement, performed at 22.7 MeV [11]: Taking the prediction based on the CD-Bonn potential as a reference, we find that here, too, the p-d data lie well below the CD-Bonn curve in the minimum, while our 80° data points are above it at all energies. (No n-d measurement could be made at 22.7 MeV because, due to the $3/2^+$ resonance in ^{5}He, no accurate data for the n-α analyzing power exist at this energy.) The difference between the p-d data and our n-d results hints at a considerable influence of the Coulomb force in the minimum of $K_y^{y'}$. In view of theoretical studies on the $3N$ system including the Coulomb force, such pronounced effects are not surprising [50]. Especially in the cross-section minimum around $\theta_{\rm lab}=80°$, interference effects can be large and a high beam energy is no counterargument because low internuclear energies are always involved. Thus p-d experiments should not be compared to n-d calculations if subtle properties of the NN interaction, like the strength of the tensor force or three-nucleon forces, are to be investigated.

As Table III shows, there exists a similar connection between P_D and the triton binding energy as there is between P_D and the minimum of $K_y^{y'}$; i.e., the larger E_t, the lower the minimum of $K_y^{y'}$. Thereby the CD-Bonn potential, which comes closest to the experimental value of $E_t^{\rm expt}=8.48$ MeV, also gives the smallest value for $K_y^{y'}|_{\rm min}$. This suggests that the addition of a 3NF which brings the individual NN force predictions into agreement with $E_t^{\rm expt}$ will also lead to an agreement in the predictions for $K_y^{y'}|_{\rm min}$ for all four potentials. We already found effects of the TM 3NF on $K_y^{y'}$ before [3,19,20].

In order to answer this question, we adjusted the cutoff parameter Λ in the form factors of the 2π-exchange TM 3NF [7] in such a way that, together with a given NN force, the experimental triton binding energy is reproduced [49]. The resulting Λ's are shown in Table IV. These results were obtained with calculations where both the NN and the $3N$ forces act within all partial waves up to $j_{\rm max}=5$; the inclusion of partial waves with $j=6$ changes E_t only by about 0.1%. Thus we now have four $3N$ model Hamiltonians to our disposal which all give the same triton binding energy.

Using these four models, we recalculated $K_y^{y'}$ at our four energies, again with $j_{\rm max}=3$. The results are depicted in Fig. 8. The 3NF causes only a small decrease at $\theta_{\rm lab}=50°$, and all four predictions still are close to the experimental values there. On average, the theory is now 3% below the data at this angle, with the best agreement at the two highest energies. At $\theta_{\rm lab}=80°$, the effect is much more pronounced. Here the predictions for $K_y^{y'}$ are decreased appreciably so that they now lie almost 10% below the experimental data points. The values of $K_y^{y'}$ at $\theta_{\rm lab}=80°$ obtained by including the 3NF's with adjusted strengths are listed in Table IV. Comparing the pure NN force predictions for $K_y^{y'}$ to those including the 3NF, we see that the strength of the 3NF needed to reproduce the experimental triton binding energy indeed gets the predictions of the four different NN potentials into close agreement with each other at all angles; only the prediction based on the local Nijm II potential lies somewhat higher than the rest, the largest difference being 2.3% in the minimum at 25.8 MeV. Thus, $K_y^{y'}$ essentially scales with the triton binding energy. The fact that a scattering observable scales with E_t is not a trivial result which is generally to be expected. We found in [3,51] that there are $3N$ scattering observables which do scale with E_t, albeit at much lower energies, and others which do not. $K_y^{y'}$ belonged to the scaling ones at 3 MeV.

TABLE IV. Cutoff parameters Λ of the TM 3NF as fitted to the triton binding energy for the various potentials and the values of $K_y^{y'}$ at $\theta_{\rm lab}=80°$ obtained with these NN and $3N$ forces.

			$K_y^{y'}(80°)$ at E_n (MeV)			
Potential	Λ/m_π	E_t (MeV)	15.0	17.0	19.0	25.8
AV18	5.215	8.479	0.585	0.549	0.524	0.498
Nijm I	5.147	8.480	0.583	0.547	0.523	0.499
Nijm II	4.990	8.477	0.593	0.558	0.534	0.510
CD-Bonn	4.856	8.483	0.582	0.546	0.521	0.496

Looking again at the p-d data [14] at 19 MeV in Fig. 8, we see that the n-d theory with 3NF's goes right through most of the data points, and a similar picture is obtained for $K_y^{y'}$ at 22.7 MeV [11] (not shown). This, however, is probably fortuitous because it is not the case for the polarization transfer parameter $K_z^{x'}$. In Fig. 9 we show the p-d data for $K_z^{x'}$, also from Ref. [14], together with the corresponding n-d predictions. One sees clearly that there is no such agreement for $K_z^{x'}$, and our caution concerning the comparison of p-d data with n-d calculations still holds true.

Considering the original aim of our experiment, the present result might be disappointing at first sight. Because the effect of the tensor force on $K_y^{y'}$ is counterbalanced by the 3NF even at our energies, nothing can be learned about the strength of the tensor force in a direct way, contrary to earlier expectations [3,11]. It must be emphasized, however, that the theoretical foundation of three-nucleon forces is still in its infancy, and the TM 3NF, with its severe cutoff dependence, is not a very realistic force. It is not derived consistently within one scheme together with the respective NN potential, but ''added'' artificially. It is therefore not too surprising that the various theoretical predictions, although agreeing with each other, do not reproduce $K_y^{y'}$ at 80°. There

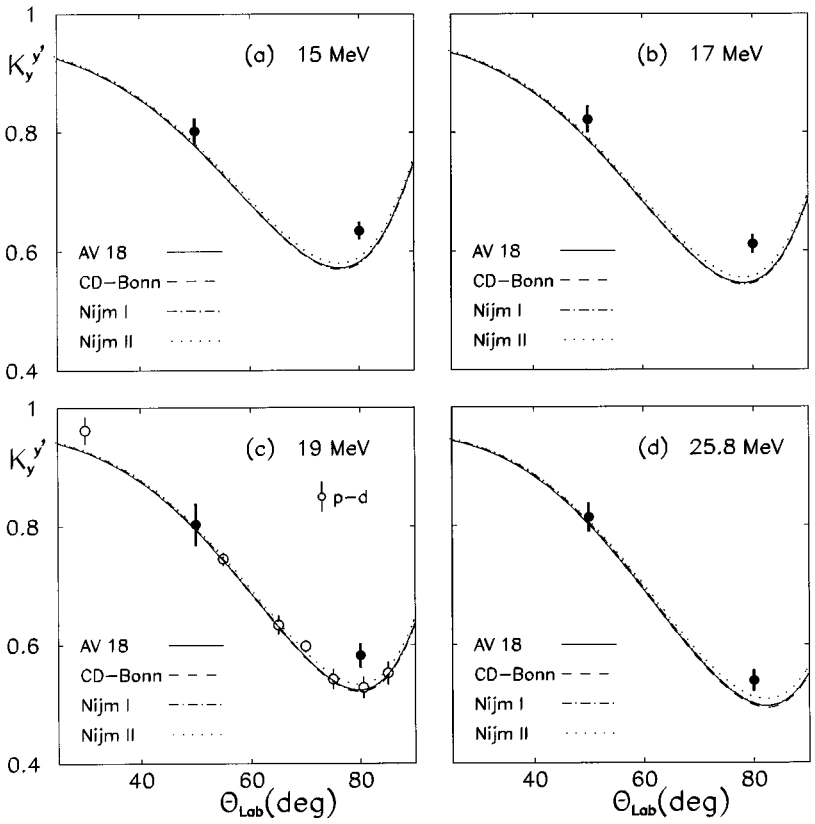

FIG. 8. Same as Fig. 7, but with the inclusion of the Tucson-Melbourne three-nucleon force, as explained in the main text.

are other examples where the theory fails to describe the experimental data, most notably the n-d analyzing powers A_y and iT_{11} [3]. Thus our data provide an additional test of future improvements in the $2N$ and $3N$ scattering theory.

VI. SUMMARY AND CONCLUSION

We have measured the nucleon-to-nucleon polarization transfer parameter $K_y^{y'}$ for the first time in neutron-deuteron scattering, at bombarding energies $E_n = 15.0$, 17.0, 19.0, and 25.8 MeV and scattering angles $\theta_{\rm lab} = 50°$ and 80°. Reaching an accuracy which approaches that of comparable p-d experiments, we now have a measurement of a second-order n-d spin observable accurate enough to serve for quantitative studies. A comparison with p-d data shows the importance of the Coulomb force at the angles around the minimum of $K_y^{y'}$ where also the cross section is very small. This is different at forward angles where our n-d data agree with the existing p-d data very well. We have to conclude that for quantitative studies p-d spin-transfer data should not be compared to n-d calculations even at higher energies.

We compared our experimental data with rigorous, fully charge-dependent Faddeev calculations in momentum space, using the four realistic and phase-equivalent NN potentials AV18, Nijm I and II, and CD-Bonn. At $\theta_{\rm lab} = 50°$, where $K_y^{y'}$ is less sensitive to details of the underlying dynamics, all four potentials predict essentially the same values for $K_y^{y'}$, in good agreement with our experimental results. In the minimum around $\theta_{\rm lab} = 80°$, the four predictions deviate from each other, the differences apparently being related to the different D-state probabilities of the four potentials.

We then added the 2π-exchange Tucson-Melbourne 3NF, which was adjusted individually for each of the four NN potentials to reproduce the triton binding energy. We found that at $\theta_{\rm lab} = 50°$ the 3NF causes only a small shift in $K_y^{y'}$, essentially preserving the agreement with experiment. At $\theta_{\rm lab} = 80°$, the shifts are larger and the theory underestimates $K_y^{y'}$ by almost 10%. However, the predictions of all four models are now in close agreement with each other over the

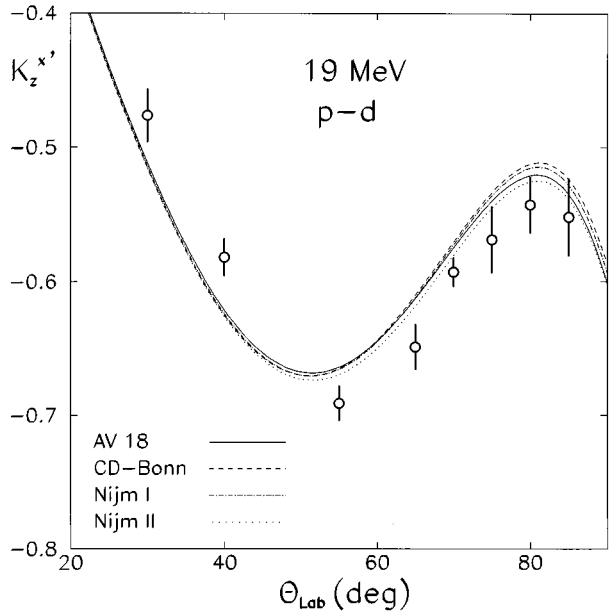

FIG. 9. Comparison of the 19-MeV p-d data for $K_z^{x'}$ [14] with the model predictions including the TM 3 NF.

whole angular range. This means that $K_y^{y'}$ scales with the triton binding energy even at energies above 20 MeV, contrary to earlier belief [3], thus precluding a decision as to which of the NN forces might be more realistic. There are other $3N$ observables which are sensitive to the tensor force, but do not scale, as we found in a recent study [3], especially the vector and tensor analyzing powers, the neutron-to-deuteron tensor spin-transfer coefficients, and the tensor spin-correlation coefficients. We therefore propose to also measure these nonscaling quantities in order to learn more about the specific details of the dynamics.

The close coincidence of the predictions of all four $3N$ model Hamiltonians, together with the disagreement between theory and experiment in the minimum of $K_y^{y'}$, is a challenge to theory. More insight into the physics and the action of $3N$ forces is required.

ACKNOWLEDGMENTS

The authors wish to thank Dr. P. D. Eversheim and Dr. P. Meyer for their expert help with the operation of the polarized ion source. They are also grateful to Dr. W. Schauerte from the Geodetic Institute for his assistance in accurately surveying the targets and detectors for this experiment. This work was supported in part by the Deutsche Forschungsgemeinschaft under Grant Nos. Wi 1144/1-1, Wi 1144/1-2, and Gl 87/19-2. The numerical calculations were performed on the Cray T90 and T3E computers of the Höchstleistungsrechenzentrum Jülich, Germany.

[1] V. G. J. Stoks, R. A. M. Klomp, M. C. M. Rentmeester, and J. J. de Swart, Phys. Rev. C **48**, 792 (1993).
[2] R. A. Arndt, I. Strakovsky, and R. L. Workman, Phys. Rev. C **50**, 2731 (1994).
[3] W. Glöckle, H. Witała, D. Hüber, H. Kamada, and J. Golak, Phys. Rep. **274**, 107 (1996).
[4] R. Machleidt, Adv. Nucl. Phys. **19**, 189 (1989).
[5] A. Stadler, W. Glöckle, and P. U. Sauer, Phys. Rev. C **44**, 2319 (1991).
[6] A. Stadler, J. Adam, Jr., H. Henning, and P. U. Sauer, Phys. Rev. C **51**, 2896 (1995).
[7] S. A. Coon, M. D. Scadron, P. C. McNamee, B. R. Barrett, D. W. E. Blatt, and B. H. J. McKellar, Nucl. Phys. **A317**, 242 (1979); S. A. Coon and W. Glöckle, Phys. Rev. C **23**, 1790 (1981).
[8] S. A. Coon and M. T. Peña, Phys. Rev. C **48**, 2559 (1993).
[9] D. Plümper, J. Flender, and M. F. Gari, Phys. Rev. C **49**, 2370 (1994); J. A. Eden and M. F. Gari, *ibid.* **43**, 1510 (1996).
[10] H. Witała, W. Glöckle, and Th. Cornelius, Nucl. Phys. **A496**, 446 (1989).
[11] M. Clajus, P. M. Egun, W. Grüebler, P. Hautle, I. Slaus, B. Vuaridel, F. Sperisen, W. Kretschmer, A. Rauscher, W. Schuster, R. Weidmann, M. Haller, M. Bruno, F. Cannata, M. D'Agostino, H. Witała, T. Cornelius, W. Glöckle, and P. A. Schmelzbach, Phys. Lett. B **245**, 333 (1990).
[12] M. Clajus, P. M. Egun, W. Grüebler, P. Hautle, W. Kretschmer, A. Rauscher, W. Schuster, R. Weidmann, M. Haller, M. Bruno, F. Cannata, M. D'Agostino, I. Slaus, P. A. Schmelzbach, B. Vuaridel, F. Sperisen, H. Witała, Th. Cornelius, and W. Glöckle, Nucl. Phys. **A508**, 261c (1990).
[13] F. Sperisen, W. Grüebler, V. König, P. A. Schmelzbach, K. Elsener, B. Jenny, C. Schweizer, J. Ulbricht, and P. Doleschall, Nucl. Phys. **A422**, 81 (1984).
[14] L. Sydow, S. Lemaitre, P. Nießen, K. R. Nyga, G. Rauprich, R. Reckenfelderbäumer, S. Vǒhl, H. Paetz gen. Schieck, H. Witała, and W. Glöckle, Nucl. Phys. **A567**, 55 (1994).
[15] R. B. Wiringa, V. G. J. Stoks, and R. Schiavilla, Phys. Rev. C **51**, 38 (1995).
[16] V. G. J. Stoks, R. A. M. Klomp, C. P. F. Terheggen, and J. J. de Swart, Phys. Rev. C **49**, 2950 (1994).
[17] V. G. J. Stoks (private communication).
[18] R. Machleidt, F. Sammarruca, and Y. Song, Phys. Rev. C **53**, 1483 (1996).
[19] D. Hüber, Ph.D. thesis, Ruhr-Universität Bochum, 1993.
[20] D. Hüber, H. Witała, and W. Glöckle, Few-Body Syst. **14**, 171 (1993).
[21] D. Hüber, H. Kamada, H. Witała, and W. Glöckle, Acta Phys. Pol. B **28**, 101 (1997).
[22] D. Hüber, H. Witała, A. Nogga, W. Glöckle, and H. Kamada, Few-Body Syst. **22**, 107 (1997).
[23] W. von Witsch and J. G. Willaschek, Nucl. Instrum. Methods **138**, 13 (1976).
[24] T. Köble, F. Meyer, M. Ockenfels, J. Weltz, W. von Witsch, and G. Wollmann, Nucl. Instrum. Methods Phys. Res. A **275**, 460 (1989).
[25] M. Hohlweck, T. Köble, F. Meyer, M. Ockenfels, J. Weltz, and W. von Witsch, Nucl. Instrum. Methods Phys. Res. A **281**, 277 (1989).
[26] M. Ockenfels, T. Köble, M. Schwindt, J. Weltz, and W. von Witsch, Nucl. Phys. **A534**, 248 (1991).
[27] Supplied by Nuclear Enterprises Technology Limited, Edinburgh, Scotland.
[28] M. Schwindt, Diplom thesis, Universität Bonn, 1990 (unpublished).
[29] Phillips Scientific, Suffern, New York 10901.
[30] G. G. Ohlsen, Rep. Prog. Phys. **35**, 717 (1972).
[31] G. G. Ohlsen and P. W. Keaton, Jr., Nucl. Instrum. Methods **109**, 41 (1973).
[32] M. Ockenfels, F. Meyer, T. Köble, W. von Witsch, J. Weltz, K. Wingender, and G. Wollmann, Nucl. Phys. **A526**, 109 (1991).
[33] P. Hempen, Ph.D. thesis, Universität Bonn, 1997.
[34] T. Cornelius, W. Glöckle, J. Haidenbauer, Y. Koike, W. Plessas, and H. Witała, Phys. Rev. C **41**, 2538 (1990).
[35] W. B. Broste, G. S. Mutchler, J. E. Simmons, R. A. Arndt, and L. D. Roper, Phys. Rev. C **5**, 761 (1972).
[36] H. Krupp, J. C. Hiebert, H. O. Klages, P. Doll, J. Hansmeyer, P. Plischke, J. Wilczynski, and H. Zankel, Phys. Rev. C **30**, 1810 (1984).
[37] Th. Stammbach and R. L. Walter, Nucl. Phys. **A180**, 225 (1972).
[38] R. A. Hardekopf and G. G. Ohlsen, Phys. Rev. C **15**, 514 (1977).

[39] M. Clajus, P. Egun, W. Grüebler, P. Hautle, A. Weber, P. A. Schmelzbach, W. Kretschmer, M. Haller, J. C. Prenzel, A. Rauscher, W. Schuster, and R. Weidmann, Nucl. Instrum. Methods Phys. Res. A **281**, 17 (1989).

[40] J. E. Bond and F. W. K. Firk, Nucl. Phys. **A287**, 317 (1977).

[41] K. Hofenbitzer, P. Clotten, P. Hempen, V. Huhn, W. Metschulat, M. Schwindt, L. Wätzold, Ch. Weber, and W. von Witsch, Phys. Rev. C (to be published); K. Hofenbitzer, Ph.D. thesis, Universität Bonn, 1997.

[42] W. Glöckle, H. Witała, and Th. Cornelius, Nucl. Phys. **A508**, 115c (1990).

[43] C. R. Howell, W. Tornow, K. Murphy, H. G. Pfützner, M. L. Roberts, Anli Li, P. D. Felsher, R. L. Walter, I. Slaus, P. A. Treado, and Y. Koike, Few-Body Syst. **2**, 19 (1987); J. Cub, E. Finkh, G. Fuchs, K. Gebhardt, K. Geißdörfer, R. Lin, and J. Strate, *ibid.* **6**, 151 (1989); W. Nitz, Diplom thesis, Universität Karlsruhe, 1985 (unpublished).

[44] Evaluated Nuclear Data File ENDF/B-VI, BNL, Upton, New York, 1996.

[45] W. Galati, J. D. Brandenberger, and J. L. Weil, Phys. Rev. C **5**, 1508 (1972); W. Tornow, J. Phys. G **9**, 1507 (1983); W. Tornow, R. L. Walter, and R. C. Byrd, *ibid.* **11**, 379 (1985).

[46] E. Woye, W. Tornow, G. Mack, C. E. Floyd, P. P. Guss, K. Murphy, R. C. Byrd, S. A. Wender, R. L. Walter, T. B. Clegg, and W. Wylie, Nucl. Phys. **A394**, 139 (1983); N. Olsson, B. Trostell, and E. Ramström, *ibid.* **A496**, 505 (1989).

[47] H. Witała, Th. Cornelius, and W. Glöckle, Few-Body Syst. **3**, 123 (1988).

[48] H. Witała, W. Glöckle, and Th. Cornelius, Phys. Rev. C **39**, 384 (1989).

[49] A. Nogga, D. Hüber, H. Kamada, and W. Glöckle, Phys. Lett. B **409**, 19 (1997).

[50] E. O. Alt (private communication).

[51] D. Hüber, H. Witała, H. Kamada, W. Glöckle, and J. Golak, *Few-Body Problems in Physics*, edited by F. Gross, AIP Conf. Proc. No. 334 (AIP, New York, 1995), p. 391; W. Glöckle, H. Witała, H. Kamada, D. Hüber, and J. Golak, in *ibid.*, p. 45.